Metrol. Meas. Syst., Vol. XVIII (2011), No. 4, pp. 583-596.

PAN POLSKA AKADEMIA NAUK

METROLOGY AND MEASUREMENT SYSTEMS

Index 330930, ISSN 0860-8229

www.metrology.pg.gda.pl

M&MS

ESTIMATION OF THE AMPLITUDE SQUARE USING THE INTERPOLATED DISCRETE FOURIER TRANSFORM

Tomaž Lušin, Dušan Agrež

University of Ljubljana, Faculty of Electrical Engineering, Tržaška 25, 1001 Ljubljana, Slovenia (✉dusan.agrez@fe.uni-lj.si)

Abstract

To improve the estimation of active power, the possibility of estimating the amplitude square of a signal component using the interpolation of the squared amplitude discrete Fourier transform (DFT) coefficients is presented. As with an energy-based approach, the amplitude square can be estimated with the squared amplitude DFT coefficients around the component peak and a suitable interpolation algorithm. The use of the Hann window, for which the frequency spectrum is well known, and the three largest local amplitude DFT coefficients gives lower systematic errors in squared interpolated approach or in better interpolated squared approach than the energy-based approach, although the frequency has to be estimated in the first step. All investigated algorithms have almost the same noise propagation and the standard deviations are about two times larger than the Cramér-Rao lower bound.

Keywords: estimation, amplitude square, spectral data processing, interpolated DFT, Hann window.

1. Introduction

Processing sampled signals in time or frequency domain for finding the selected signal parameter is nowadays common practice in measurement. In many estimation applications in the field of electrical power systems, the component amplitude, its square and consequently the active power of the sinusoidal signal must be known with high accuracy [1]. The adopted estimation procedures can be classified as either time-domain (parametric) [2-4] or frequency-domain (nonparametric) methods [4-7]. Parametric procedures are model-based and require computationally intensive algorithms to determine the coefficients of the model that fits the available data. On the other hand, the model order issue does not apply when using nonparametric techniques, which estimate the parameters of interest by first evaluating the discrete Fourier transform (DFT) of the digitized signal and then the suitable parameter (frequency, amplitude and phase) of each spectral tone. Moreover, nonparametric techniques exhibit a lower computational effort due to the availability of fast Fourier transform (FFT) algorithms and are more robust. However, such advantages are achieved at the expense of decreased frequency selectivity and statistical efficiency. Since the selectivity and efficiency reduction can be compensated for by respectively increasing the observation interval length or the number of samples analyzed, frequency-domain based estimation methods can be widely applied.

The main drawback of the frequency-domain methods is the well-known leakage effect due to non-coherent sampling [8]. Assuming non-coherency in the sampling process, spectral granularity and leakage may adversely affect the accuracy of the estimation process. To cope

Article history: received on Sept. 23, 2011; received in revised form on Nov. 22, 2011; accepted on Nov. 23, 2011; available online on Dec. 12, 2011.

with such issues, various methods have been devised for the accurate estimation of tone amplitudes and their squares [9], and among them two main methods are frequently used: the energy-based method estimates the power in each spectral component by evaluating the total energy falling inside a band including the window main lobe [8, 10], and the interpolated DFT estimates the amplitude of the spectral lines of interest using two or more neighboring DFT coefficients, starting from those centered in each spectrum's local maximum [11-13]. While the energy-based method is a more intuitive technique and only needs generic window specifications, the interpolated WDFT requires more calculations and a thorough knowledge of spectral window behavior but performs with a reduced systematic bias error as shown in this paper. The interpolated DFT estimation procedure for the amplitude square can be improved by interpolation – suitable summation – of the squared amplitude DFT coefficients around the investigated component. The paper proposes and discusses algorithms to improve the estimation of the amplitude square for the active power of electrical systems under non-coherent sampling conditions. It is based on smoothing sampled data by windowing, prior to their numeric integration, and then averaging the squared amplitude DFT coefficients to reduce the leakage effects.

The basic measuring principle of the numerical-based wattmeters is the equally spaced simultaneous sampling of voltage $u(k)$ and current $i(k)$ with the sampling frequency f_s. The active power is usually estimated by averaging of the instantaneous power $p(k)=u(k)\cdot i(k)$:

$$\overline{P}=\frac{1}{N}\sum_{k=0}^{N-1}u(k)\cdot i(k) \qquad k=0,\ldots,N-1 \tag{1}$$

or expressed by $M+1$ frequency components:

$$\overline{P}=U_0I_0+\sum_{m=1}^{M}U_mI_m\cos(\varphi_{m,u}-\varphi_{m,i}) \tag{2}$$

where U_0 and I_0 represent the DC voltage and current components. The effective values of the other voltage and current components are $U_m=A_{m,u}/\sqrt{2}$ and $I_m=A_{m,i}/\sqrt{2}$.

Estimation of the particular power component $U_mI_m\cos(\varphi_{m,u}-\varphi_{m,i})$ requires the estimation of the sine-wave amplitude A_m and phase φ_m. For both estimations in the direct approach, the frequency as the basic parameter has to be estimated first. If one rewrites the equation for one component

$$\frac{A_{m,u}\cdot A_{m,i}}{2}\cos(\varphi_{m,u}-\varphi_{m,i})=A_{m,i}^2\frac{A_{m,u}}{2A_{m,i}}\cos(\varphi_{m,u}-\varphi_{m,i}), \tag{3}$$

it can be noticed that three quantities have to be estimated: the square of the amplitude, the amplitude quotient and the phase difference. The last two quantities can be estimated without knowing the frequency if the simultaneousness of the sampling on both channels is assumed, and the measurement time of the signals is the same [14]. However, the problem remains of the sine-wave power estimation or better the square of the amplitude A_m^2 estimation.

As mentioned previously, the two main groups of methods used for estimating the square of the amplitude are the energy-based method [10], without knowledge of the frequency, and the non-parametric approach by the interpolation of the DFT amplitude coefficients [7], where the frequency has to be estimated first.

The key step for the second group of the estimations is the determination of the position along the frequency axis of the measured component δ_m between the two largest local DFT

coefficients $G(i)$ and $G(i+1)$ surrounding the component itself (Fig. 1). The sampled analog multi-frequency signal $g(t)$ can be written as follows:

$$g(k\Delta t)_N = w(k)\cdot\sum_{m=0}^{M} A_m \sin(2\pi f_m k\Delta t + \varphi_m). \tag{4}$$

Using N samples of signal (1), the DFT at the spectral line i is given by

$$G(i) = -\frac{j}{2}\sum_{m=0}^{M} A_m\left[W(i-\theta_m)e^{j\varphi_m} - W(i+\theta_m)e^{-j\varphi_m}\right], \tag{5}$$

where θ_m is the signal frequency divided by the frequency resolution of the time window $\Delta f = 1/(N\Delta t)$ and can be written in two parts:

$$\theta_m = \frac{f_m}{\Delta f} = i_m + \delta_m \qquad -0.5 < \delta_m \le 0.5, \tag{6}$$

where i_m is an integer value, and the displacement term δ_m is caused by non-coherent sampling.

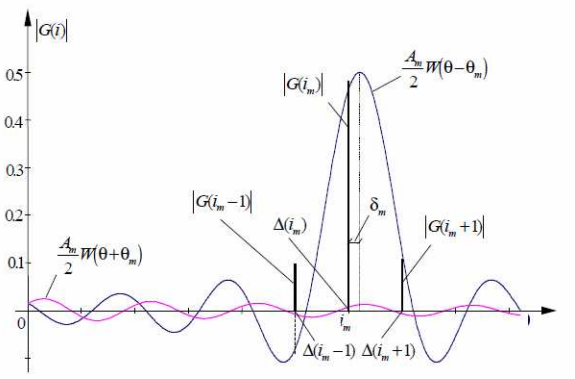

Fig. 1. Leakage influence of the negative part of the sine spectrum with rectangular window at the positive part of the spectrum (i_m=6).

The amplitude coefficients surrounding one component in the signal are due to the short-range leakage contribution of the window spectrum weighted by the amplitude of the frequency component (from the first term in (5)), and the long-range leakage contributions (from both terms in (5)). Therefore, these coefficients can be written in two parts (7-9): the larger term due to the short-range spectrum leakage of the component investigated m, and bias $|\Delta(i)|$ due to the long-range leakage of the spectral image of this component (Fig. 1) and also due to the long-range leakage contributions from other components in the multi-component signal.

$$\begin{aligned}|G(i_m-1)| &= \frac{A_m}{2}\left|W(1+\delta_m)e^{j\varphi_m} - W(2i_m+\delta_m-1)e^{-j\varphi_m}\right| + \sum_{k=0,k\neq m}^{M}|\Delta(i_k)| \\ &= \frac{A_m}{2}|W(1+\delta_m)| \mp |\Delta(i_m-1)|\end{aligned} \tag{7}$$

$$\begin{aligned}|G(i_m)| &= \frac{A_m}{2}\left|W(\delta_m)e^{j\varphi_m} - W(2i_m+\delta_m)e^{-j\varphi_m}\right| + \sum_{k=0,k\neq m}^{M}|\Delta(i_k)| \\ &= \frac{A_m}{2}|W(\delta_m)| \pm |\Delta(i_m)|\end{aligned} \tag{8}$$

$$\begin{aligned}|G(i_m+1)| &= \frac{A_m}{2}\left|W(1-\delta_m)e^{j\varphi_m} - W(2i_m+\delta_m+1)e^{-j\varphi_m}\right| + \sum_{k=0,k\neq m}^{M}|\Delta(i_k)| \\ &= \frac{A_m}{2}|W(1-\delta_m)| \mp |\Delta(i_m+1)|\end{aligned} \tag{9}$$

In the case of non-coherent sampling ($\delta_m \neq 0$), the portions $|\Delta(i)|$ of the long-range leakage tails have the following properties: they decrease with increasing frequency and they change sign at successive coefficients $|G(i)|$, if they have a sine function in the kernel ($\sin(\pi(i+\delta_m)) = -\sin(\pi(i\pm 1+\delta_m))$). For example, the rectangular window, the Hann window, and the Rife-Vincent Class I windows, satisfy this condition. For the sake of analytical simplicity, cosine-class windows are frequently used [12]. Windows of class RV-I are designed for maximization of window spectrum side-lobes fall-off θ^{-p} [15]:

$$w(k) = \sum_{l=0}^{p-1}(-1)^l a_{l,1}\cdot\cos\left(l\frac{2\pi}{N}\cdot k\right),\ k=0,\ldots,N-1. \tag{10}$$

When the order p is 1 (RV1-1), the coefficient $a_{0,1}$ is 1 and equation (10) gives a rectangular shape. If p is 2 ($\mathrm{RV1-2}: a_{0,1}=1/2, a_{1,1}=1/2$) and we get the Hann window. Higher values of p expand the window transform main-lobe and reduce the spectral leakage.

2. Energy-Based Method

In the energy-based methods, the power of the sine wave is evaluated by using a small number of DFT samples centred at the spectrum peak which is located in the frequency bin i_m. In particular, for *p*-term cosine windows, it has been shown that the use of $(2p+1)$ DFT samples is advantageous since it ensures a very good compromise between the selectivity capability of the nearby spectral components and spectral leakage reduction [10]. The power of the sine-wave amplitude A_m^2 is estimated as:

$$A_m^2 = 4\frac{\sum_{i=i_m-r}^{i_m+r}|G(i)|^2}{NNPG},\ r_{\text{optimal}} = p, \tag{11}$$

where $NNPG$ is the window Normalized Noise Power Gain [16], defined as

$$NNPG = \frac{1}{N}\sum_{k=0}^{N-1}w^2(k),\ NNPG_{\text{Hann}} = 0{,}375. \tag{12}$$

We checked the error of the amplitude square estimation $e(A^2) = A^2/A^{2*} - 1$ (A^{2*} is the true value of the amplitude square) for one sine component in the signal with a double scan varying both frequency and phase ($A_m = 1;\ N = 1024;\ 1 \le \theta \le 6,\ \Delta\theta = 0.001$ and $-\pi/2 \le \varphi \le \pi/2,\ \Delta\varphi = \pi/18$). The absolute maximum values of the errors (from 19

iterations) at the given relative frequency were compared with the Hann window for different multi-point estimations (11).

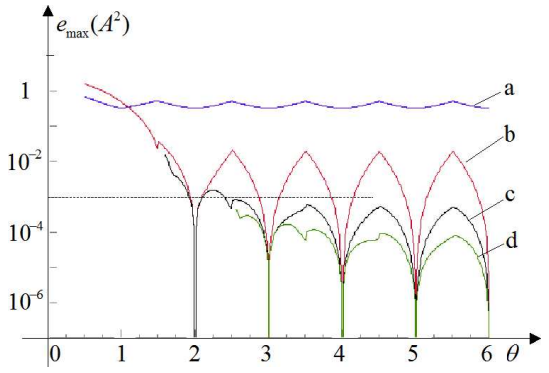

Fig. 2. Maximal relative values of errors of the amplitude square estimation by (11) and the Hann window: a – the one-point est. (r=0), b – the three-point est. (r=1), c – the five-point est. ($r_{optimal}$=2), d – the seven-point est. (r=3).

When the 'optimal' five-point estimation is used we are sure to reach the limit of 10^{-3} in the relative value of the error at $\theta_m \geq 2.4$.

3. Interpolated DFT Method

The second group of the estimations of the amplitude square has two main possibilities: estimation of the component amplitude by interpolation of the DFT and after that squaring of the result, and the second approach is by interpolation of the squared DFT amplitude coefficients. Both approaches need the estimation of the displacement first and a window with a well-defined spectrum.

When the Hann window is used, for which the spectrum $|W_{\mathrm{H}}(\theta)|_{N>>1} = |\sin(\pi\theta)| / |2\pi\theta(1-\theta^2)|$ is analytically known, all three coefficients of the maximum have the same sign (the main lobe is extended to four frequency resolution intervals $4\Delta f$) and they can be expressed as:

$$|W_{\mathrm{H}}(\delta_m)| \cong \frac{\sin(\pi\delta_m)}{2\pi\delta_m(1-\delta_m^2)}, \tag{13}$$

$$|W_{\mathrm{H}}(1+\delta_m)| \cong \frac{\sin(\pi(1+\delta_m))}{2\pi(1+\delta_m)[1-(1+\delta_m)^2]} = \frac{\sin(\pi\delta_m)}{2\pi\delta_m(1+\delta_m)(2+\delta_m)}, \tag{14}$$

$$|W_{\mathrm{H}}(1-\delta_m)| \cong \frac{\sin(\pi\delta_m)}{2\pi\delta_m(1-\delta_m)(2-\delta_m)}. \tag{15}$$

For the five-point estimations, it is also useful to express the next nearby amplitude DFT coefficients:

$$\begin{aligned} |W_{\mathrm{H}}(2+\delta_m)| &\cong \frac{\sin(\pi(2+\delta_m))}{2\pi(1+\delta_m)[1-(2+\delta_m)^2]} \\ &= \frac{-\sin(\pi\delta_m)}{2\pi(1+\delta_m)(2+\delta_m)(3+\delta_m)} \end{aligned} \tag{16}$$

$$\left|W_{\mathrm{H}}(2-\delta_m)\right| \cong \frac{\sin(\pi\delta_m)}{2\pi(1-\delta_m)(2-\delta_m)(3-\delta_m)}. \tag{17}$$

The displacement term can be expressed as a function of the quotient of the amplitude coefficients by the interpolated DFT [7]:

$$\delta_{m\mathrm{H}} \cong 2\cdot\frac{\left(\left|G(i_m+1)\right|-\left|G(i_m-1)\right|\right)}{\left|G(i_m-1)\right|+2\left|G(i_m)\right|+\left|G(i_m+1)\right|}. \tag{18}$$

An alternative way to estimate the displacement is the energy-based method approach without knowledge of the window spectrum used (19) [5], but systematic errors are larger than in the case of interpolated DFT using the Hann window (Fig. 3).

$$\delta_{\mathrm{EBM,H}} \cong \frac{\sum_{i=i_m-r}^{i_m+r}(i-i_m)\left|G(i)\right|^2}{\sum_{i=i_m-r}^{i_m+r}\left|G(i)\right|^2},\ \theta = i_m+\delta_{\mathrm{EBM,H}}. \tag{19}$$

The errors of the relative frequency estimations $E(\theta)=\theta-\theta^*$ (θ^* is the true value of the frequency) were checked for one sine component in the signal, as in Fig. 2 (Fig. 3: $A_m=1$; $N=1024$; a double scan varying both frequency and phase: $1\le\theta\le 6$, $\Delta\theta=0.001$ and $-\pi/2\le\varphi\le\pi/2$, $\Delta\varphi=\pi/18$). The absolute maximum values of the errors (from 19 iterations) at the given relative frequency were compared with the Hann window ((19) and (18)) for different multi-point estimations.

Fig. 3 shows that the estimation by three-point DFT interpolation (18) gives better results than EBM interpolation (19), even when using seven points after 4.5 cycles in the measurement interval $4.5\le\theta$.

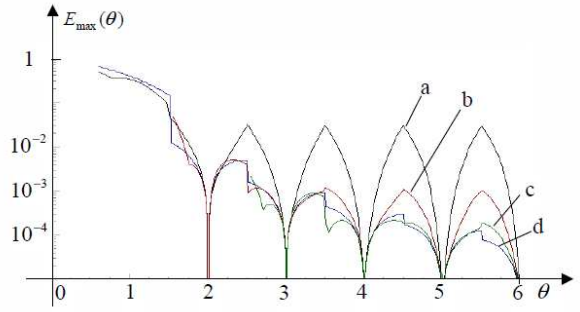

Fig. 3. Maximal absolute values of errors of the relative frequency estimation with the multi-point DFT interpolations for the Hann window: a – the three-point EBM est. (19) $r=1$, b – the five-point EBM est. (19) $r_{\mathrm{optimal}}=2$, c – the seven-point EBM est. (19) $r=3$, d - the three-point DFT interpolation (18).

When the displacement δ_m for the specific component is determined, it is easy to obtain the amplitude for the Hann window from (8) and (13) for the one-point estimation ${}_1A_m^*$, if the long-range contribution $\left|\Delta(i_m)\right|$ is neglected:

$${}_1A_m \cong 2\frac{\left|G(i_m)\right|}{\left|W_{\mathrm{H}}(\delta_m)\right|} = 2\left|\frac{2\pi\delta_m(1-\delta_m^2)}{\sin(\pi\delta_m)}\right|\left|G(i_m)\right|, \tag{20}$$

$$ {}_1A_m^2 \cong 4\frac{|G(i_m)|^2}{|W_{\mathrm{H}}(\delta_m)|^2}. \tag{21} $$

In this manner, we can obtain the amplitude by summing the largest three local DFT coefficients around the signal component [7]:

$$ \begin{aligned} \left[|G(i_m-1)|+2|G(i_m)|+|G(i_m+1)|\right] &= \frac{A_m}{2}\left[|W(1+\delta_m)|\pm|\Delta(i_m-1)|+\right. \\ &\left.+2|W(\delta_m)|\mp 2|\Delta(i_m)|+|W(1-\delta_m)|\pm|\Delta(i_m+1)|\right] \end{aligned} $$

$$ A_m \cong 2\cdot\frac{\left[|G(i_m-1)|+2|G(i_m)|+|G(i_m+1)|\right]}{|W(1+\delta_m)|+2|W(\delta_m)|+|W(1-\delta_m)|}. \tag{22} $$

Using the Hann window (equations (13), (14), and (15)):

$$ \begin{aligned} &|W_{\mathrm{H}}(1+\delta_m)|+2|W_{\mathrm{H}}(\delta_m)|+|W_{\mathrm{H}}(1-\delta_m)| = \\ &\quad = \frac{\sin(\pi\delta_m)}{2\pi\delta_m}\frac{12}{(1-\delta_m^2)(4-\delta_m^2)} = |W_{\mathrm{H}}(\delta_m)|\frac{12}{(4-\delta_m^2)}, \end{aligned} $$

the amplitude square estimation with the three-point interpolation ($ {}_3A_m^*$) can be expressed as follows:

$$ {}_3A_{m\mathrm{H}}^2 \cong 4\frac{\left[|G(i_m-1)|+2|G(i_m)|+|G(i_m+1)|\right]^2}{12^2|W_{\mathrm{H}}(\delta_m)|^2/(4-\delta_m^2)^2}. \tag{23} $$

We can use the same procedure for the five-point interpolation ($ {}_5A_m^*$) with ten subtractions of the tails [7]:

$$ \begin{aligned} {}_5A_{m\mathrm{H}}^2 &= \frac{1}{|W_{\mathrm{H}}(\delta_m)|^2}\frac{(4-\delta_m^2)^2(9-\delta_m^2)^2}{180^2}\cdot \\ &\cdot\left[6|G(i_m)|+4\left(|G(i_m+1)|+|G(i_m-1)|\right)+\left||G(i_m+2)|-|G(i_m-2)|\right|\right]^2. \end{aligned} \tag{24} $$

The relative error drops with increasing relative frequency and with the number of the interpolation points (Fig. 4; the simulation procedure is the same as in Fig. 2). Comparing Figures 2 and 4 shows the reduction in the systematic errors in the interpolated DFT procedure.

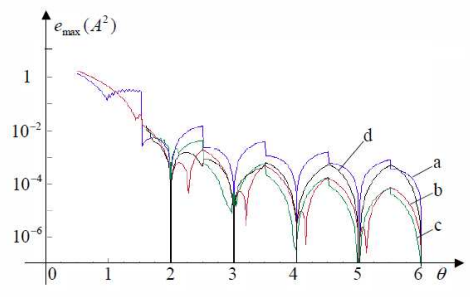

Fig. 4. Maximal relative values of errors of the amplitude power estimation with the multi-point DFT interpolations for the Hann window (θ is obtained with the three-point interpolation (18)): a – the one-point est. (21), b – the three-point est. (23), c – the five-point est. (24), d – the five-point EBM est. (11).

4. Interpolated Squared DFT Method

As in the EBM approach, the amplitude square can be estimated with the squared amplitude DFT coefficients and the use of a suitable interpolation algorithm. For interpolation we need at least two amplitude DFT coefficients (the largest and the second largest DFT coefficients)

$$|G(i_m)| = \frac{A_m}{2}|W(\delta_m)| \pm |\Delta(i_m)|, \tag{25}$$

$$|G(i_m + s)| = \frac{A_m}{2}|W(1-\delta_m)| \mp |\Delta(i_m + s)|, \tag{26}$$

where s is the sign of displacement $\delta_m \geq 0 \rightarrow s = +1$, $\delta_m < 0 \rightarrow s = -1$.

Squaring and summing the coefficients give the following expressions:

$$|G(i_m)|^2 = \frac{A_m^2}{4}|W(\delta_m)|^2 \pm 2\frac{A_m}{2}|W(\delta_m)| \cdot |\Delta(i_m)| + |\Delta(i_m)|^2, \tag{27}$$

$$|G(i_m + s)|^2 = \frac{A_m^2}{4}|W(1-\delta_m)|^2 \mp A_m|W(1-\delta_m)| \cdot |\Delta(i_m + s)| + |\Delta(i_m + s)|^2, \tag{28}$$

$$\begin{aligned} |G(i_m)|^2 + |G(i_m + s)|^2 = {} & \frac{A_m^2}{4}\left(|W(\delta_m)|^2 + |W(1-\delta_m)|^2\right) \\ & \pm A_m\left(|W(\delta_m)| \cdot |\Delta(i_m)| - |W(1-\delta_m)| \cdot |\Delta(i_m + s)|\right). \\ & + |\Delta(i_m)|^2 + |\Delta(i_m + s)|^2 \end{aligned} \tag{29}$$

Since the squared long-range leakage contributions are negligible $|\Delta(i_m)|^2 + |\Delta(i_m + s)|^2 << \frac{A_m^2}{4}\left(|W(\delta_m)|^2 + |W(1-\delta_m)|^2\right)$ and the difference in the second part is also very small $\left(|W(\delta_m)| \cdot |\Delta(i_m)| - |W(1-\delta_m)| \cdot |\Delta(i_m + s)|\right) << 1$, the amplitude square can be estimated by:

$${}_2A_m^2 \doteq 4\frac{|G(i_m)|^2 + |G(i_m + s)|^2}{|W(\delta_m)|^2 + |W(1-\delta_m)|^2} = \frac{4}{|W(\delta_m)|^2}\frac{|G(i_m)|^2 + |G(i_m + s)|^2}{1 + \left(\frac{|W(1-\delta_m)|}{|W(\delta_m)|}\right)^2}. \tag{30}$$

Using the Hann window (equations (13) and (15)) the quotient of the used coefficients gives

$$\frac{|W_{\mathrm{H}}(1-\delta_m)|}{|W_{\mathrm{H}}(\delta_m)|} = \frac{2\pi\delta_m(1-\delta_m^2)}{\sin(\pi\delta_m)} \cdot \frac{\sin(\pi\delta_m)}{2\pi\delta_m(1-\delta_m)(2-\delta_m)} = \frac{1+\delta_m}{2-\delta_m} \tag{31}$$

and from here:

$${}_{2a}A_{m\mathrm{H}}^2 \doteq \frac{4}{|W_{\mathrm{H}}(\delta_m)|^2} \cdot \frac{|G(i_m)|^2 + |G(i_m + s)|^2}{1 + \left(\frac{1+\delta_m}{2-\delta_m}\right)^2}. \tag{32}$$

Increasing the number of the amplitude DFT coefficients used improves the amplitude square estimation. For the three-point estimation, the three largest local amplitude DFT coefficients should be used:

$$\left|G(i_m-1)\right|^2=\frac{A_m^2}{4}\left|W\left(1+\delta_m\right)\right|^2\mp A_m\left|W\left(1+\delta_m\right)\right|\cdot\left|\Delta\left(i_m-1\right)\right|+\left|\Delta\left(i_m-1\right)\right|^2, \tag{33}$$

$$\left|G(i_m)\right|^2=\frac{A_m^2}{4}\left|W\left(\delta_m\right)\right|^2\pm A_m\left|W\left(\delta_m\right)\right|\cdot\left|\Delta\left(i_m\right)\right|+\left|\Delta\left(i_m\right)\right|^2, \tag{34}$$

$$\left|G(i_m+1)\right|^2=\frac{A_m^2}{4}\left|W\left(1-\delta_m\right)\right|^2\mp A_m\left|W\left(1-\delta_m\right)\right|\cdot\left|\Delta\left(i_m+1\right)\right|+\left|\Delta\left(i_m+1\right)\right|^2. \tag{35}$$

Summation of the squared coefficients

$$\begin{aligned}&\left|G(i_m-1)\right|^2+\left|G(i_m)\right|^2+\left|G(i_m+1)\right|^2=\\&=\frac{A_m^2}{4}\left(\left|W\left(1+\delta_m\right)\right|^2+\left|W\left(\delta_m\right)\right|^2+\left|W\left(1-\delta_m\right)\right|^2\right)\\&\pm A_m\left(-\left|W\left(1+\delta_m\right)\right|\cdot\left|\Delta\left(i_m-1\right)\right|+\left|W\left(\delta_m\right)\right|\cdot\left|\Delta\left(i_m\right)\right|-\left|W\left(1-\delta_m\right)\right|\cdot\left|\Delta\left(i_m+1\right)\right|\right)\\&+\left|\Delta\left(i_m-1\right)\right|^2+\left|\Delta\left(i_m\right)\right|^2+\left|\Delta\left(i_m+s\right)\right|^2\end{aligned} \tag{36}$$

gives the possibility to estimate the amplitude square if the leakage tails are neglected $\left|\Delta\left(i_m-1\right)\right|^2+\left|\Delta\left(i_m\right)\right|^2+\left|\Delta\left(i_m+s\right)\right|^2<<1$ and considering that the second part in (36) is close to zero $\left[-\left|W\left(1+\delta_m\right)\right|\cdot\left|\Delta\left(i_m-1\right)\right|+\left|W\left(\delta_m\right)\right|\cdot\left|\Delta\left(i_m\right)\right|-\left|W\left(1-\delta_m\right)\right|\cdot\left|\Delta\left(i_m+1\right)\right|\right]\approx 0$. The expression of the amplitude square estimation is close to the expression for the energy-based estimation (11), except the denominator is a suitable summation of the largest window coefficients instead of *NNPG*:

$$A_m^2\doteq 4\frac{\left|G(i_m-1)\right|^2+\left|G(i_m)\right|^2+\left|G(i_m+1)\right|^2}{\left|W\left(1+\delta_m\right)\right|^2+\left|W\left(\delta_m\right)\right|^2+\left|W\left(1-\delta_m\right)\right|^2} \tag{37}$$

Using the Hann window, the quotient of the used coefficients $\left|W_{\mathrm{H}}\left(1+\delta_m\right)\right|/\left|W_{\mathrm{H}}\left(\delta_m\right)\right|$ (equations (13) and (14)) can be expressed as:

$$\frac{\left|W_{\mathrm{H}}\left(1+\delta_m\right)\right|}{\left|W_{\mathrm{H}}\left(\delta_m\right)\right|}=\frac{2\pi\delta_m\left(1-\delta_m^2\right)}{\sin\left(\pi\delta_m\right)}\cdot\frac{\sin\left(\pi\delta_m\right)}{2\pi\delta_m(1+\delta_m)(2+\delta_m)}=\frac{1-\delta_m}{2+\delta_m} \tag{38}$$

and the amplitude square can be estimated without the value of the displacement sign:

$${}_3A_{m\mathrm{H}}^2\doteq\frac{4}{\left|W_{\mathrm{H}}\left(\delta_m\right)\right|^2}\cdot\frac{\left|G(i_m-1)\right|^2+\left|G(i_m)\right|^2+\left|G(i_m+1)\right|^2}{\left[1+\left(\frac{1+\delta_m}{2-\delta_m}\right)^2+\left(\frac{1-\delta_m}{2+\delta_m}\right)^2\right]} \tag{39}$$

The five-point estimation of the amplitude square can follow the same procedure using two more DFT coefficients ((16) and (17)):

$$\begin{aligned}{}_5A_{m\mathrm{H}}^2\doteq&\frac{4}{\left|W_{\mathrm{H}}\left(\delta_m\right)\right|^2}\cdot\\&\cdot\frac{\left|G(i_m-2)\right|^2+\left|G(i_m-1)\right|^2+\left|G(i_m)\right|^2+\left|G(i_m+1)\right|^2+\left|G(i_m+2)\right|^2}{\left[1+\left(\frac{1+\delta_m}{2-\delta_m}\right)^2+\left(\frac{1-\delta_m}{2+\delta_m}\right)^2+\left(\frac{\delta_m(1+\delta_m)}{(2-\delta_m)(3-\delta_m)}\right)^2+\left(\frac{\delta_m(1-\delta_m)}{(2+\delta_m)(3+\delta_m)}\right)^2\right]}\end{aligned} \tag{40}$$

It can be noticed (Fig. 5) that suitable summations in the denominators of the estimation equations (32), (39), and (40) reduce the systematic errors, especially in the regions where the displacement is $0 < \delta_m < 0.5$. This is even further visible if we compare the three-point estimations (Fig. 6).

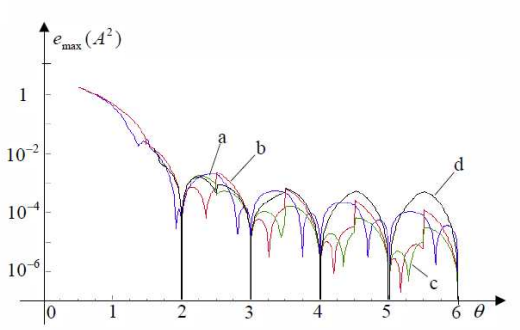

Fig. 5. Maximal relative values of errors of the amplitude square estimation with the multi-point DFT interpolations for the Hann window (θ is obtained with the three-point interpolation (18): a – the two-point est. (32), b – the three-point est. (39), c – the five-point est. (40), d – the five-point EBM est. (11).

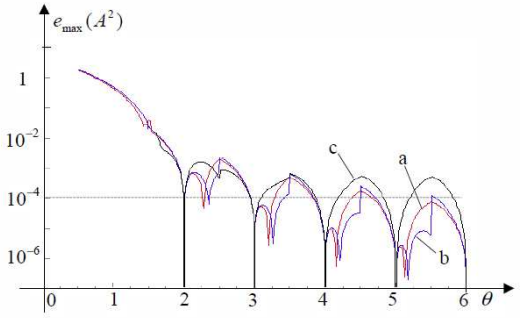

Fig. 6. Maximal relative values of errors of the amplitude square estimation with the three-point DFT interpolations for the Hann window (θ is obtained with the three-point interpolation (18): a – the IDFT est. (23), b – the squared DFT est. (39), c – the five-point EBM est. (11).

5. The Influence of Noise on Estimations

The reduction of systematic errors increases the contribution of the noise random part of errors. The quantization error is a minimum that has to be taken into consideration in the measurement uncertainty of the final result. In simulations, the white noise with a rectangular distribution, zero mean and standard deviation $\sigma_t = A_{\text{noise}} / \sqrt{3}$ was added to the signal in the time domain. The corresponding signal-to-noise ratio in the time domain was $SNR = A^2 / (2\sigma^2)$. At every test point of frequency and phase change, as in Fig. 2, 50 trials of random added noise were used for the estimation of the amplitude square standard deviation (Fig. 7: at every frequency altogether $19 \cdot 50 = 950$ trials). Noise propagation in the algorithms was compared to the Cramér-Rao lower bound [17] (Fig. 7).

$$\sigma_{\text{CRB}}(A^2) \cong A^2 \sqrt{\frac{2}{N\ SNR}} \tag{41}$$

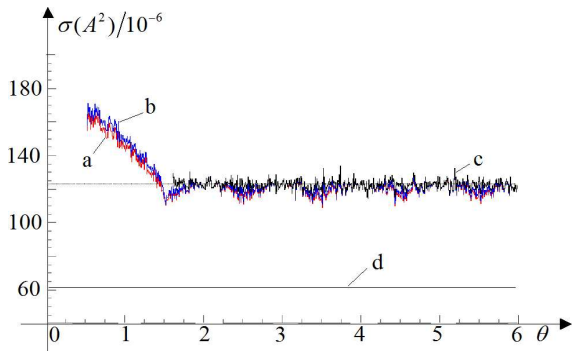

Fig. 7. The standard deviations of errors of the amplitude square estimation with the three-point DFT interpolations for the Hann window (θ is obtained with the three-point interpolation (18)): a – the IDFT est. (23), b – the squared DFT est. (39), c – the five-point EBM est. (11), d – the CRB bound $\sigma_{\mathrm{CRB}}\left(A^2\right)=62.5\cdot10^{-6}$ (41), signal: $A=1$, $\sigma_{\mathrm{noise}}=0.001$, $SNR=5\cdot10^5$ (57 dB).

The lowest standard deviation is with the IDFT estimations. At relative frequencies larger than $\theta_m \geq 1.5$ the standard deviations are about two times larger than the Cramér-Rao lower bound (Fig. 7d). It is useful to analyze both contributions together (systematic and noise) searching for the maximal errors at each relative frequency (Fig. 8). In those regions where the displacement is $0<\delta_m<0.5$, the proposed three-point estimations using the Hann window give better results than the energy-based method.

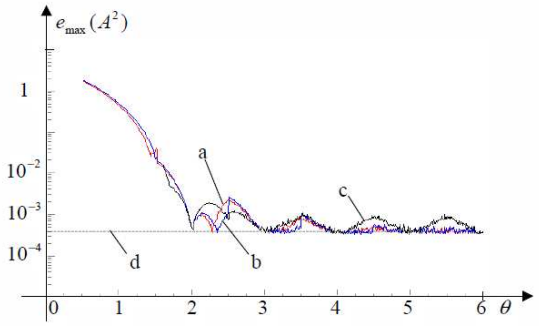

Fig. 8. Maximal relative values of errors of the amplitude square estimation with the three-point DFT interpolations for the Hann window (θ is obtained with the three-point interpolation (18)): a– the IDFT est. (23), b – the squared DFT est. (39), c – the five-point EBM est. (11), d – the expected maximal value of the estimations $\langle e_{\max}\rangle \approx 3\cdot\left(2\cdot\sigma_{\mathrm{CRB}}\left(A^2\right)\right)\approx 4\cdot10^{-4}$, signal: $A=1$, $\sigma_{\mathrm{noise}}=0.001$, $SNR=5\cdot10^5$ (57 dB).

6. Experimental Results

The proposed method has been validated on a real measurement system. First, for the simulation of the single component signal, a waveform generator was used (HP3245A: $\hat{u}=1\,\mathrm{V}$, noise $U_{\mathrm{noise}}\approx10\,\mu\mathrm{V_{RMS}}$, frequency resolution $0.001\,\mathrm{Hz}$, frequency accuracy $\pm5\cdot10^{-5}$) and for data acquisition a sampling voltmeter (Agilent 34411A: $U_{\mathrm{Range}}=1\,\mathrm{V}$, $U_{\mathrm{noise}}\approx30\cdot10^{-6}\cdot U_{\mathrm{Range}}=30\,\mu\mathrm{V_{RMS}}$, $f_{\mathrm{sampling}}=50\,\mathrm{kHz}$, $N=1000$) was synchronized. The testing procedure was the same as in Figs. 7 and 8. As expected, according to specifications, the effective value of the noise floor in this experiment was $U_{\mathrm{noise}}\approx32\,\mu\mathrm{V_{RMS}}$ and all

algorithms show almost the same level of noise error contribution at the three cycles, and more in the measurement interval (Fig. 9d). The EBM approach presents slightly worse results at lower values of the relative frequency $\theta < 3$.

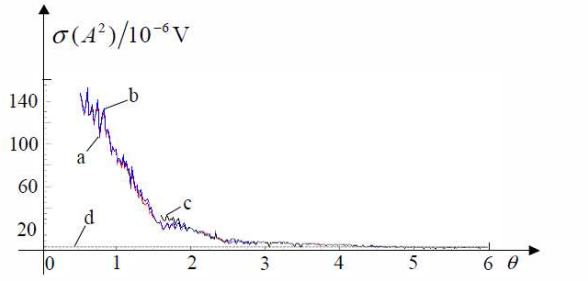

Fig. 9. The experimental standard deviations of errors of the amplitude square estimations with the three-point DFT interpolations for the Hann window (θ is obtained with the three-point interpolation (18)): a – the IDFT est. (23), b – the squared DFT est. (39), c – the five-point EBM est. (11), d – $\sigma_{\mathrm{est}}(A^2) \approx 4 \cdot 10^{-6}\,\mathrm{V} \rightarrow \sigma_{\mathrm{CRB}}(A^2) \approx 2 \cdot 10^{-6}\,\mathrm{V}$ (41), signal: $A \doteq 1\,\mathrm{V}$, $\sigma_{\mathrm{noise}} \doteq 32\,\mu\mathrm{V}$, $SNR = 5 \cdot 10^8$ (87 dB).

The experiment also confirms the behavior of the maximal errors in regions where the displacement is $0 < \delta_m < 0.5$ (Fig. 10). The proposed three-point estimations using the Hann window give better results than EBM.

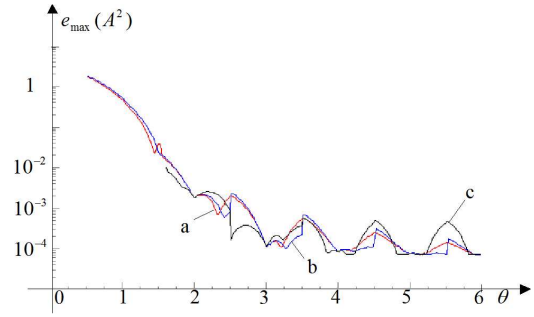

Fig. 10. Maximal relative values of errors of the amplitude square estimation in experiment using the Hann window (θ is obtained with the three-point interpolation (18)): a– the IDFT est. (23), b – the squared DFT est. (39), c – the five-point EBM est. (11).

To evaluate the estimation algorithms in the case of a multi-component signal we also tested them by a triangular shape signal from the signal generator (HP3245A: $\hat{u}_{\mathrm{triang}} = 1\,\mathrm{V}$). In the test, like in Fig. 10 and $2 \le \theta_1 \le 6$, the maximal error of the squared amplitude of the third component was searched (Fig. 11). The amplitude of this component is nine times lower then the fundamental one ($A_3 = A_1/9 = (\hat{u} \cdot 8/\pi^2)/9 = 0.09\,\mathrm{V}$ and power is $A_3^2 = 8.11\,\mathrm{mV}$) and the leakage error contribution increases.

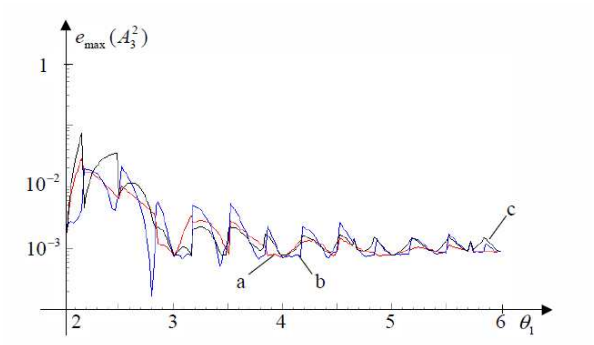

Fig. 11. Maximal relative values of errors of the squared amplitude of the third component in experiment using the triangular shape signal (θ is obtained with the three-point interpolation (18)): a– the IDFT est. (23), b – the squared DFT est. (39), c – the five-point EBM est. (11).

In the case of the third harmonic component of the triangular-shaped signal, the maximal errors are larger but the interpolated squared DFT approach gives the lowest errors, especially in the regions where the relative frequency is $2h/6 < \delta_m < (2h+1)/6$ ($h = 0, 1, 2$) as can be expected for the three-times larger relative frequency of the third signal component.

7. Conclusion

In this paper, the advantages of the squared DFT interpolations for the amplitude square estimation are presented and compared with the interpolated DFT and the energy-based approach. In the analyses the Hann window is used, for which the frequency spectrum is well known and is a good compromise between the width of the main-lobe and the side-lobes fall-off. The use of the three largest local amplitude DFT coefficients gives lower systematic errors in the squared interpolated approach or in the interpolated squared approach than in the energy-based approach, although the frequency has to be estimated in the first step. Comparing the interpolated algorithms, the interpolated squared approach gives the lowest systematic error and it is more than ten times lower than in the case of the energy-based approach in those regions where the displacement is $0 < \delta_m < 0.5$. All algorithms investigated have almost the same noise propagation, and the standard deviations are about two times larger than the Cramér-Rao lower bound.

References

[1] Emanuel, A.E. (2004). Summary of IEEE Standard 1459: Definitions for the measurement of electric power quantities under sinusoidal, nonsinusoidal, balanced or unbalanced conditions. *IEEE Transactions on Industry Applications*, 40(3), 869-876.

[2] Stoica, P., Li, H., Li, J. (2000). Amplitude Estimation of Sinusoidal Signals: Survey, New Results, and an Application. *IEEE Transactions on Signal Processing*, 48(2), 338-352.

[3] Cataliotti, A., Cosentino, V., Nuccio, S. (2008). A virtual instrument for the measurement of IEEE Std 1459-2000 power quantities. *IEEE Transactions on Instrumentation and Measurement*, 57(1), 85 -94.

[4] Novotný, M., Slepička, D., Sedláček, M. (2007). Uncertainty Analysis of the RMS Value and Phase in the Frequency Domain by Noncoherent Sampling. *IEEE Transactions on Instrumentation and Measurement*, 56(3), 983-989.

[5] Offelli, C., Petri, D. (1990). A frequency-domain procedure for accurate real-time signal parameter measurement. *IEEE Transactions on Instrumentation and Measurement*, 39, 363-368.

[6] Carbone, P., Nunzi, E., Petri, D. (2001). Windows for ADC Dynamic Testing via Frequency-Domain Analysis. *IEEE Transactions on Instrumentation and Measurement*, 50(6), 1571-1576.

[7] Agrež, D. (2002). Weighted Multi-Point Interpolated DFT to Improve Amplitude Estimation of Multi-Frequency Signal. *IEEE Transactions on Instrumentation and Measurement*, 51, 287-292.

[8] Solomon, O.M. (1994). The Use of DFT Windows in Signal-to-Noise ratio and Harmonic Distortion Computation. *IEEE Transactions on Instrumentation and Measurement*, 43(2), 194-199.

[9] Sedlacek, M., Stoudek, Z. (2011). Active power measurements - An overview and a comparison of dsp algorithms by noncoherent sampling, *Metrology and Measurement Systems*, 18(2), 173-184.

[10] Petri, D. (2002). Frequency-domain testing of waveform digitizers. *IEEE Transactions on Instrumentation and Measurement*, 51, 445-453.

[11] Grandke, T. (1983). Interpolation Algorithms for Discrete Fourier Transforms of Weighted Signals. *IEEE Transactions on Instrumentation and Measurement*, IM-32(2), 350-355.

[12] Andria, G., Savino, M., Trotta, A. (1989). Windows and interpolation algorithms to improve electrical measurement accuracy. *IEEE Transactions on Instrumentation and Measurement*, 38(8), 856-863.

[13] Schoukens, J., Pintelon, R., Van hamme, H. (1992). The Interpolated Fast Fourier Transform: A Comparative Study. *IEEE Transaction on Instrumentation and Measurement*, 41, 226-232.

[14] Agrež, D. (2010). Estimation of parameters of two sine signals with common frequency. In *Proceedings of the IEEE I^{2}MTC/2010*, Austin, USA, 67-72.

[15] MsC. Siebert, W. (1986). *Circuits, Signals, and Systems*, The MIT Press, Cambridge, Massachusetts.

[16] Harris, F.J. (1978). On the Use of Windows for Harmonic Analysis with the Discrete Fourier Transform. *Proceedings of the IEEE*, 66(1), 51-83.

[17] Händel, P. (2008). Parameter estimation employing a dual-channel sine-wave model under a Gaussian assumption. *IEEE Transactions on Instrumentation and Measurement,* 57(8), 1661-1669.